

**ORIGINAL PAPER****The isolated elliptical galaxy NGC 5812 - MOND or Dark Matter? †**Tom Richtler<sup>1</sup> | Ricardo Salinas<sup>2</sup> | Richard Lane<sup>3</sup> | Michael Hilker<sup>4</sup><sup>1</sup>Departamento de Astronomía, Universidad de Concepción, Concepción, Chile<sup>2</sup>Departamento de Astronomía, Universidad de La Serena, Av. Juan Cisternas 1200 Norte, La Serena, Chile<sup>3</sup>Centro de Investigación en Astronomía, Universidad Bernardo O'Higgins, Avenida Viel 1497, Santiago, Chile<sup>4</sup>European Southern Observatory, Karl-Schwarzschildstr. 2, 85748, Garching, Germany**Correspondence**

Tom Richtler Email: tom@astro-udec.cl

arXiv:2311.12598v1 [astro-ph.GA] 21 Nov 2023

There exist isolated elliptical galaxies, whose dynamics can be modelled without resorting to dark matter or MOND, e.g. NGC 7507. Such objects lack understanding within the current framework of galaxy formation. The isolated elliptical NGC 5812 is another object to investigate a possible role of isolation. We use globular clusters (GCs) and the galaxy light itself as dynamical tracers to constrain its mass profile. We employ Gemini/GMOS mask spectroscopy, apply the GMOS reduction procedures provided within IRAF, measure GC velocities by cross correlation methods and extract the line-of-sight kinematics of galaxy spectra using the tool pPXF. We identify 28 GCs with an outermost galactocentric distance of 20 kpc, for which velocities could be obtained. Furthermore, 16 spectra of the integrated galaxy light out to 6 kpc have been used to model the central kinematics. These spectra provide evidence for a disturbed velocity field, which is plausible given the disturbed morphology of the galaxy. We construct spherical Jeans models for the galaxy light and apply tracer mass estimators for the globular clusters. With the assumptions inherent to the mass estimators, MOND is compatible with the mass out to 20 kpc. However, a dark matter free galaxy is not excluded, given the uncertainties related to a possible non-sphericity and a possible non-equilibrium state. We find one globular cluster with an estimated mass of  $1.6 \times 10^7 M_{\odot}$ , the first Ultra Compact Dwarf in an isolated elliptical. We put NGC 5812 into the general context of dark matter or alternative ideas in elliptical galaxies. The case for a MONDian phenomenology also among early-type galaxies has become so strong that deviating cases appear astrophysically more interesting than agreements. The baryonic Tully Fisher relation (BTFR) as predicted by MOND is observed in some samples of early-type galaxies, in others not. However, in cases of galaxies that deviate from the MONDian prediction, data quality and data completeness are often problematic.

**KEYWORDS:**

Galaxies: individual: NGC 5812 – Galaxies: kinematics and dynamics – Galaxies: star clusters

**1 | INTRODUCTION**

"Galaxies are embedded in halos of dark matter (DM) that assemble through cosmological structure formation." This

statement is the core of the present paradigm of galaxy formation in a "concordant" universe (Ostriker & Steinhardt, 1995). The most influential description of this concordant universe is found in the  $\Lambda$ CDM cosmological parameters from the Planck satellite analyses (Planck Collaboration et al., 2014), where the baryonic density parameter  $\Omega_{baryon}$  is 0.04 and the matter density parameter  $\Omega_{matter}$  is 0.3 (uncertainties and model

†Based on observations obtained with Gemini-South, Cerro Pachon, Chile, under the programme GS-2013A-Q-051.

dependencies are omitted for simplicity), if a Friedmann cosmological model is assumed. Therefore, under this paradigm dark matter (DM) plausibly consists of non-baryonic particles (Bertone, 2010; Bertone, Hooper, & Silk, 2005). Their non-detections can be understood as a crisis in the understanding of the DM concept (Bertone & Tait, 2018). However, dark matter particles might be detected in future terrestrial experiments or by observing DM annihilation products (Cherenkov Telescope Array Consortium et al., 2019; Silverwood, Weniger, Scott, & Bertone, 2015). See also Bertone and Hooper (2018) for an historical account of the dark matter concept. Currently, the tension between the locally measured Hubble constant and the Hubble constant derived from Planck data, as well as other tensions between cosmological data sets, cast doubt on the very Friedmann concept of a homogeneous universe (e.g. Di Valentino, Melchiorri, and Silk 2020, Heinesen and Buchert 2020).

This "standard cosmology" has never been accepted by the entire community. A series of papers (J. Bekenstein & Milgrom, 1984; Milgrom, 1983a, 1983b, 1983c) marked the beginning of an alternative view onto the mass discrepancy which became known as Modified Newtonian Dynamics (MOND). Dynamical features in local galaxies are difficult to reconcile with the nature of dark matter as weakly interacting massive particles (Famaey & McGaugh, 2013, 2012; Kroupa, 2015). Of particular interest is the (predicted by Milgrom) intimate relation between the baryonic matter and dark matter that has become known as the MONDian phenomenology manifest in rotation curves and in the baryonic Tully-Fisher relation of spiral galaxies (Famaey & McGaugh, 2013, 2012; Kroupa, 2015; Lelli, McGaugh, Schombert, Desmond, & Katz, 2019; McGaugh, Lelli, & Schombert, 2016).

The knowledge regarding the dynamics of *early-type galaxies* is naturally poorer because of the missing disk symmetry. Using globular clusters and planetary nebulae as dynamical tracers at larger radii as well as the hydrostatics of the hot halo gas, some elliptical galaxies have been shown to be consistent with MONDian behaviour (Lelli, McGaugh, Schombert, & Pawlowski, 2017; Milgrom, 2012; Schuberth et al., 2012; Weijmans et al., 2008). However, central galaxies in galaxy clusters apparently need an additional dark component to explain their kinematics (Richtler et al., 2011, 2008) as it is the case with entire galaxy clusters (Angus, Famaey, & Buote, 2008; Pointecouteau & Silk, 2005; Sanders, 2003) (but see the remarks in Section 7.3.1).

There is a class of early-type galaxies showing a radial behaviour of the velocity dispersion that has been dubbed "Keplerian decline" (it is of course not a Keplerian potential), meaning that models can work without a dark component (Romanowsky et al., 2003). One of Romanowsky et al.'s prominent objects is NGC 3379, which one may rank among

the dynamically best known elliptical galaxies. de Lorenzi et al. (2009) demonstrate that the available data are consistent with a variety of dynamical models and dark matter abundances. However, to permit a cosmologically motivated dark halo, a very strong radial anisotropy of the galaxy's stellar orbits is demanded, which so far has never been observed. In this context, isolated ellipticals are particularly interesting because the assembly history of their dark halos was not disturbed by a cluster or group environment (see Richtler, Salinas, Lane, Hilker, and Schirmer 2015 for a brief introduction into the literature on isolated ellipticals). As an example, we mention NGC 7507 as an even more convincing galaxy with a "Keplerian" behaviour of the velocity dispersion of the integrated galaxy light (Lane, Salinas, & Richtler, 2015; Salinas, Richtler, Bassino, Romanowsky, & Schuberth, 2012).

In this paper we show and interpret kinematical data for another isolated elliptical, NGC 5812. The globular cluster system and the galaxy's morphology in the Washington system has been studied by Lane, Salinas, and Richtler (2013). NGC 5812 is, judging from its photometric properties, an intermediate-age early-type galaxy, showing deviations from a smooth light distribution that plausibly are the relics of previous infall/interaction processes. A companion with a tidal tail is the obvious manifestation of a present galaxy-galaxy interaction.

The heliocentric radial velocity of NGC 5812 is 1970 km/s (NED). We adopt a distance of 28 Mpc ( $m-M = 32.24$ ) (Lane et al., 2013). At this distance, 1'' corresponds to 135.7 pc.

## 2 | OBSERVATIONS AND DATA REDUCTION

### 2.1 | Observations

The observations were performed in queue mode during the period May 6th to August 6th 2013 at the Gemini South Observatory at Cerro Paranal, Chile (programme GS-2013A-Q-51, PI:Richtler). The Gemini Multi-Object Spectrograph South (GMOS-S) was used. The disperser was the B600+\_G532 grism, giving a resolution of  $\sim 4.7\text{\AA}$  FWHM. The detector was a mosaic of three CCDs. In  $2\times$  binned mode, the pixel scale is  $0.15''$  and the total field of view  $5.5' \times 5.5'$ .

Three spectroscopic masks were exposed, two of them centred on NGC 5812, while the third mask was shifted by  $2.73'$  to the North. The observations are summarized in Table 1. Table entries are the mask number, the coordinates, exposure time, seeing, total number of slits, Gemini exposure coding (which gives the date), and the Universal Time of the exposure start.

| Mask | Center Position<br>(J 2000) |          | Exp. Time<br>(sec) | Seeing | # Slits | OB Id          | UT<br>(start) |
|------|-----------------------------|----------|--------------------|--------|---------|----------------|---------------|
| 1    | 15:00:55                    | -7:27:26 | 1400               | 0'9    | 37      | S20130506S0089 | 6:07          |
| 1    | 15:00:55                    | -7:27:26 | 1400               | 0'9    | 37      | S20130506S0092 | 6:34          |
| 1    | 15:00:55                    | -7:27:26 | 1400               | 0'8    | 37      | S20130506S0095 | 7:00          |
| 1    | 15:00:55                    | -7:27:26 | 1400               | 0'8    | 37      | S20130603S0078 | 3:16          |
| 1    | 15:00:55                    | -7:27:26 | 1400               | 0'8    | 37      | S20130603S0081 | 3:42          |
| 1    | 15:00:55                    | -7:27:26 | 1400               | 0'8    | 37      | S20130603S0084 | 4:09          |
| 2    | 15:00:55                    | -7:27:26 | 1430               | 0'9    | 47      | S20130605S0138 | 0:39          |
| 2    | 15:00:55                    | -7:27:26 | 1430               | 0'8    | 47      | S20130605S0144 | 5:12          |
| 2    | 15:00:55                    | -7:27:26 | 1400               | 0'9    | 47      | S20130807S0025 | 0:13          |
| 2    | 15:00:55                    | -7:27:26 | 1400               | 1'1    | 47      | S20130807S0028 | 0:13          |
| 2    | 15:00:55                    | -7:27:26 | 1400               | 1'2    | 47      | S20130807S0031 | 1:06          |
| 2    | 15:00:55                    | -7:27:26 | 1400               | 1'0    | 47      | S20130810S0038 | 0:21          |
| 3    | 15:00:55                    | -7:24:10 | 1070               | 0'8    | 22      | S20130702S0072 | 2:36          |
| 3    | 15:00:55                    | -7:24:10 | 1070               | 0'9    | 22      | S20130702S0075 | 2:58          |
| 3    | 15:00:55                    | -7:24:10 | 1070               | 1'1    | 22      | S20130702S0078 | 3:19          |
| 3    | 15:00:55                    | -7:24:10 | 1500               | 0'9    | 22      | S20130806S0075 | 1:10          |
| 3    | 15:00:55                    | -7:24:10 | 1500               | 0'8    | 22      | S20130806S0080 | 1:41          |
| 3    | 15:00:55                    | -7:24:10 | 1500               | 0'6    | 22      | S20130806S0082 | 2:12          |

**TABLE 1** List of mask characteristics.

## 2.2 | Mask preparation

Preimaging of the three fields (see Fig.1 ) was carried out on February 2013. Each field was observed in the r\_G0326-filter for 30.5 seconds. For the candidate selection we used the photometry in the Washington system by Lane et al. (2013). Cluster candidates had to fulfill the following criteria: the allowed color range was  $0.9 < C - R < 2.1$ , which is the appropriate color range for old GCs (e.g. Dirsch et al. 2003). Moreover, the candidates should exhibit a star-like appearance on the pre-images to distinguish them from background galaxies. The slit lengths were chosen by the contrasting demands to sample as many GC candidates as possible (short slits), but also allow to measure the galaxy light and the sky with sufficient accuracy (long slits). In total we set 107 slits with lengths between  $2''$  and  $15''$ . All slits have the same width of  $1''$ .

The mask design has been performed with the GEMINI software gmmms.

## 2.3 | Reductions of the GMOS masks and radial velocity measurements

The tools for the reduction were taken from the GMOS package of IRAF.

For the meaning of the IRAF/GMOS commands, we refer the reader to the IRAF manual<sup>1</sup>. The result is a multi-extension fits file with each slit being an extension.

The reduction procedure and the measurement of radial velocities has been already described in numerous other papers, e.g. Richtler et al. (2004); Schuberth et al. (2006, 2010, 2012), and here we provide a short summary.

For basic reduction, spectrum extraction and wave-length calibration, we used the IRAF-task *identify* and *apall*.

The radial velocities have been determined using the cross-correlation IRAF-task *fxcor*. Due to the very different appearance and S/N of the spectra, it turned out to be impossible to establish a standard procedure, which would always use the same task parameters. Regarding the cross-correlation interval, we found the interval 4700Å-5400 Å to produce the best results. Clearly defined correlation peaks are connected with uncertainties around 20-30 km/s. In the case of faint sources, more than one peak might appear, depending on the exact wavelength interval, within which the correlation is done. In these cases, we tested which peak was the most stable against variations of the cross-correlation interval. We used as templates a high S/N spectrum of NGC 1396, obtained with the same instrumentation during an earlier run (Richtler et al., 2004) and a spectrum of one of the brightest globular clusters in NGC 4636 (Schuberth et al., 2010).

<sup>1</sup>www.iraf.net

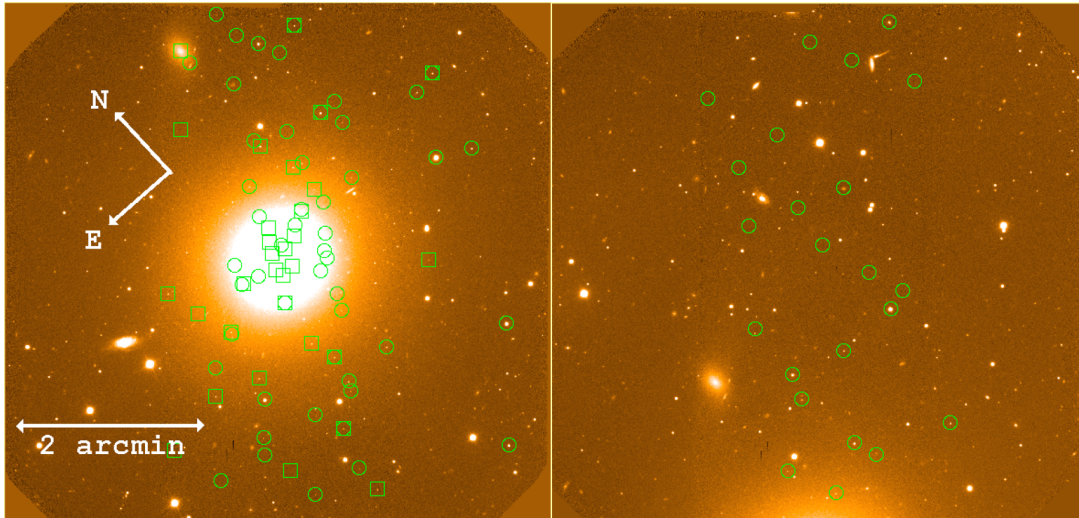


**FIGURE 1** Left panel: Slit positions for mask 1 (squares) and mask 2 (circles), overlaid on a GEMINI preimage for this run. The brightest globular cluster is the bright object 1.5' north-west of the centre. Right panel: slit positions for mask 3, overlaid on a Gemini preimage

The globular cluster data are presented in Appendix A.

### 3 | RADIAL VELOCITIES OF GLOBULAR CLUSTERS

#### 3.1 | The velocity sample

The tables A1, A2 and A3 (appendix) list all measured velocities for the galaxy light, for 29 GCs and 19 stars, respectively. The velocities derived from the two templates are listed differently to mediate an impression of the template's significance.

#### 3.2 | Systemic velocity

The systemic velocity of NGC 5812 is 1970 km/s, according to the NED. Defining our systemic velocity as the mean of the galaxy velocities and the globular cluster velocities, we end up with a somewhat lower value. The mean value and its mean uncertainty of the globular cluster velocities is  $1922 \pm 22$  km/s (from table A2). The galaxy velocities have a mean value of  $1927 \pm 7$  km/s (from table A1), which is excellent agreement. We therefore adopt 1925 km/s as the systemic velocity of NGC 5812. The reason for the difference to the NED values remains obscure.

#### 3.3 | Velocity distribution of globular clusters and estimation of virial mass

The standard deviation of the entire GC sample is  $129 \pm$  km/s, including the outlier at 1510 km/s (object 128 in Table A2). Without it the standard deviation shrinks to 109 km/s. The

maximum likelihood dispersion estimator of Pryor and Meylan (1993) that also respects the individual uncertainties, gives  $91 \pm 14$  km/s.

A Gauss fit with a fixed central value of  $v_r = 1925$ , which gives less weight to outliers, results in  $\sigma = 115 \pm 28$  km/s, where  $\sigma$  is the dispersion of the Gaussian. This Gaussian is shown as the dashed line in Fig. 2. The central part is not well fitted. A Wilkinson-Shapiro test for normality gives a p-value of 0.09 and thus does not provide a convincing argument against a normal distribution. However, the kurtosis of the velocity sample is 4.30, characterising a distribution that is more peaked than a Gaussian which physically could indicate a radial bias. More precise statements are not possible due to the small number of GCs.

A first mass estimation can be tried by inserting the dispersion into the virial theorem (e.g. Binney and Tremaine 2008, equation 4-80)

$$m_{\text{virial}} = 2.5 \times r_{\text{half}} \times \sigma^2 / G \quad (1)$$

where  $r_{\text{half}}$  is the half-mass radius and  $G = 0.0043$  (constant of gravitation in units of solar mass, km/s, and parsec). The half-mass radius is not well determined. Adopting 50 kpc as the radius of the galaxy, the half-mass radius, according to our model (see section 5.1), is 8.3 kpc,  $\sigma = 115$  km/s and the corresponding mass is  $6.4 \times 10^{10} M_{\odot}$ . The resulting mass-to-light ratio is  $M/L_R = 1.05$ , much too low for an old/intermediate-age population. A more detailed dynamical analysis arrives at more reasonable values (see section 5.2).

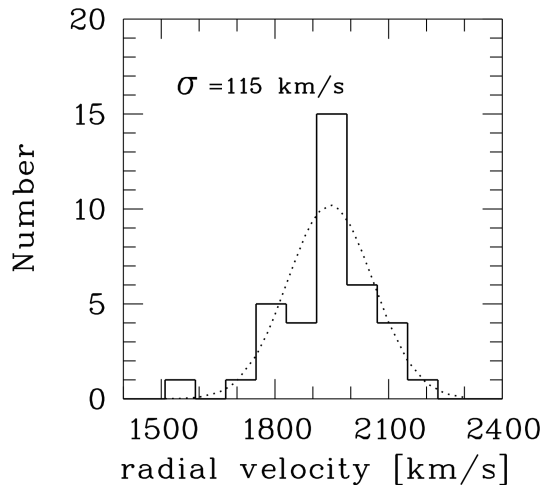


**FIGURE 2** The velocity distribution of globular clusters. The dashed line represents the fit of a Gaussian with a dispersion of 115 km/s.

### 3.4 | Colour-magnitude diagram and colour distribution

Fig.3 shows the CMD of our GC sample with available photometry. The left panel displays the observed colours and magnitudes, for the dereddened colours and absolute magnitude of the right panel, the following numbers apply. The foreground reddening, according to the NED, is  $E(B-V) = 0.076$ . The absorption in R is 0.19 mag and the reddening in C-R is  $1.97 \times E(B-V) = 0.15$  mag (Harris & Cantnera, 1977). These numbers and the distance modulus  $m-M=32.23$  are used for the calculation of the absolute magnitudes in the right panel of Fig.3. Given a specific frequency of  $S_N = 1.2$  (Lane et al., 2013), which is very low for an elliptical galaxy, it may look surprising to find so many bright GCs. Particularly striking is the bright object with  $M_R = -12.2$  mag (see caption Fig.1). As will be shown later (see section 4.2) through the analysis of the stellar M/L-ratio, NGC 5812 is dominated by light from intermediate-age populations. Many GCs are therefore expected to have higher luminosities than their old counterparts of the same mass. Comparison with the colour distribution of (Lane et al., 2013) shows that our GCs sample the full colour interval. A further hint to intermediate-age clusters is the fact that there appear clusters with  $C-R \approx 0.9$  which is too blue for old clusters even with very low metallicities.

In the upper panel of Fig.4, C-R colours are plotted versus radial velocities.

### 3.5 | A UCD in an isolated elliptical

There is one strikingly bright object among our GC sample (see caption of Fig.3). Unfortunately, the designation Ultra-compact Dwarf has become common for GCs brighter than  $M_V = -11$  or with  $R_{eff}$  larger than 10 pc, although there is no evidence that these objects share galaxy properties (see the introduction in Fahrion et al. 2019). We combined one spectrum from mask 1 and one from mask 2. The S/N of this combined spectrum (see the appendix for the spectrum) is sufficiently high to permit an analysis. We use the python version of the Penalized Pixel-Fitting (pPXF) method to extract the kinematics and population parameters (if possible) for our spectra. pPXF was first described by Cappellari and Emsellem (2004) and has been upgraded by Cappellari (2017), to which the reader is referred for details of the fitting procedure. pPXF uses the MILES stellar population library (Vazdekis et al., 2010).

pPXF returns a mass-weighted age of 12 Gyr and a mass-weighted metallicity of  $[M/H] = -0.5$ . With these values, one would expect a colour of  $C-R = 1.72$  according to the Padua models (Bressan et al., 2012), while we measure a dereddened colour of  $C-R = 1.50$ . Uncertainties in the analysis, the applied foreground reddening, the photometric calibration, and the stellar models and the photometric transformations let a difference of 0.2 mag appear not surprising. A safe statement may be that it is an old and moderately metal-poor object. Adopting the above values for age and metallicity, the models give  $M/L_R = 4.4$  (with a Chabrier IMF) and the mass follows as  $1.6 \times 10^7 M_\odot$ . This object is unfortunately not on any HST image. On Fig.2 of Lane et al. (2013) one observes that this object might be associated to a stream, but independent observations are demanded before any strong conclusion can be drawn.

### 3.6 | The companion

The companion of NGC5812 forms a long tidal tail testifying to its proximity to NGC 5812 (Lane et al., 2013). It is nucleated and of early-type. A Washington colour  $C-R = 1.33$  is typical for an old, moderately metal-poor population. The nucleus is not distinguishable in colour from the bulk of the stellar population. We put a slit of length  $5''$  on the dwarf galaxy, but S/N turned out to be insufficient for a population study. The radial velocity is 1665 km/s, differing by -260 km/s from the systemic velocity. The circular velocity at this projected distance  $2.5'$  (20.3 kpc) is between 190 km/s (stellar mass only) and 270 km/s (MONDian expectation) and therefore we expect the dwarf on its orbit to be near its pericenter.

in Fig.2 of Lane et al. (2013), one notes the distinct loop of the northern tail that indicates a change of the tail's direction. The easiest explanation would be a projection from a part

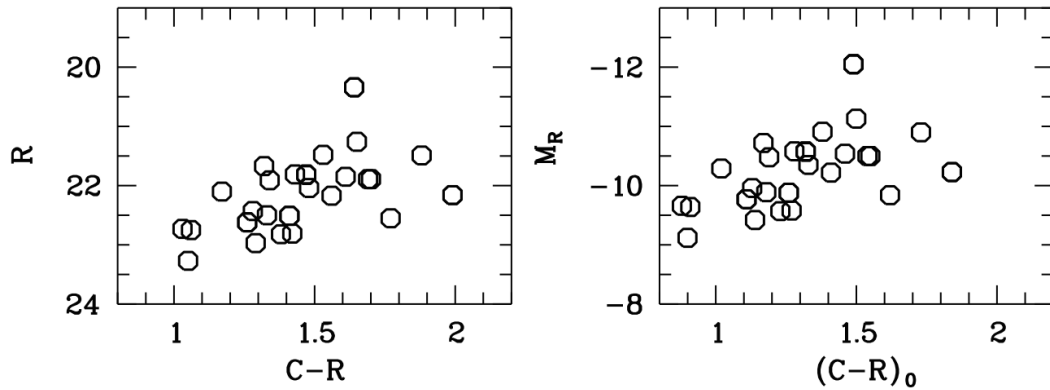


**FIGURE 3** Left panel: The colour-magnitude diagram of globular clusters with measured velocities. Right panel: Extinction and reddening corrected and with absolute magnitudes.

of the orbit before the apocentre onto the part after the apocentre. This would suggest the northern arm to be the trailing arm and the southern arm to be the leading arm. As Lane et al. (2013) note, the plurality of tidal features might be the debris of previous orbits of the companion.

Our spectra do not show emission lines, consistent with the possibility that the dwarf never picked up interstellar gas so that young or intermediate-age populations do not exist.

See the discussion section for more remarks.

## 4 | THE GALAXY SPECTRA

We put 17 slits on the galaxy itself in mask 1 and mask 2. To enable sky subtraction, we put sky slits at large galactocentric radii to ensure minimal galaxy contamination. Because the spectral range changes with the frame x-coordinate, we made sure that a given galaxy slit finds its sky slit with the corresponding spectral range. The slit locations are given in Table A1.

### 4.1 | The galaxy slits and their kinematical information

pPXF offers the possibility to fit 4 moments of the shapes of the absorption lines: the velocity, the velocity dispersion, the skewness, and the kurtosis (see e.g. section 6.2 of Schuberth et al. 2010). The latter two higher moments describe the asymmetric and symmetric deviations from Gaussianity and are expressed by the respective coefficients of Gauss-Hermite polynomials (e.g. van der Marel and Franx 1993). Fitting only the first two moments is more appropriate, given the limited S/N, but we performed both fits with four moments without

using the higher moments for any analysis. The velocity dispersion in case of fitting four moments is significantly smaller by about 20-30 km/s. The question is what is the "correct" dispersion? The velocity distribution whose second moments enters the Jeans-equation is a pure Gaussian only in the case of an isothermal density profile in connection with isotropy. In Fig.6, we show both sets of measured velocity dispersions. The radial velocities (the heliocentric correction is only -0.2 km/s for mask 1) are given in Table A1.

### 4.2 | Stellar populations

Constraining the population parameters age and metallicity allows to constrain the stellar mass-to-light ratio, assuming the shape of the stellar mass function. The GC spectra, due to their low signal-to-noise, are not suitable for such analyses. Only the brightest globular cluster and some spectra near the galaxy centre have a suitable brightness. For those objects, the results of the population synthesis using pPXF are listed in Table A1. A metallicity gradient is apparent with the central spectra being similar to solar metallicity, spectra at larger radii showing lower metallicities typically of  $[Fe/]=-0.3$ . A linear regression gives  $[M/H] = -0.1 * R[kpc] + 0.083$ . A difference in age cannot be seen. All spectra indicate a very old age. Because the pPXF-ages are older than the standard age of the universe (they are not cosmologically calibrated), we simply adopt 12 Gyr. Fig.8 of Lane et al. (2013) shows that the reality of this metallicity gradient is supported by the colour gradient which exists within  $50''$  (6.8 kpc).

That means that also the M/L of the stellar population shows a gradient and that models with mass-follows-light may be doubtful even in absence of dark matter.

The webtool CMD3.6 (<http://stev.oapd.inaf.it/cgi-bin/cmd-3.6>) provides theoretical M/L-values in many photometric

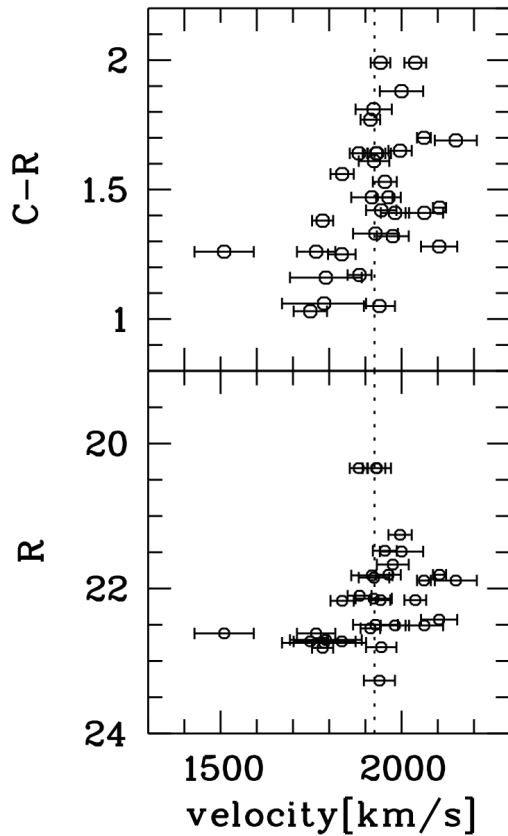


**FIGURE 4** Upper panel: Colour C-R vs. radial velocity for all slits. Lower panel: R-magnitudes vs. radial velocities for all slits. The vertical dotted line is the systemic velocity of NGC 5812.

systems (among other things), offering a rich parametrisation. With default parameters and a Chabrier log-normal stellar mass function, one gets the following  $M/L$ -values in the R-band: For an age of 12 Gyr and solar metallicity,  $M/L_R = 5.1$ , for an age of 12 Gyr and  $[M/H] = -0.4$ ,  $M/L_R = 4.2$ . For these values, we adopted the absolute magnitude of the sun as  $M_R = 4.43$  (Willmer, 2018).

## 5 | DYNAMICS OF NGC 5812

### 5.1 | A revised photometric model

Our photometric model from Lane et al. (2013), where we fitted the brightness profile with a double beta-model with exponents -1.7 and -0.9, was thought to be a very good spherical representation of the light distribution. Unfortunately, the measurements have a calibration error that results in a model which is too bright in R by 0.45 mag. It has, moreover, a

practical disadvantage in that it does not permit a closed analytical formula of the three-dimensional cumulative luminosity, which is useful in numerical integration of Jeans models. Therefore we use in this work a corrected formula, which is as good in describing the profile, but is a simple beta-model with -1 as the exponent. Using the photometric data from Lane et al. (2013) (their Table A.2.) the surface brightness then is

$$\mu(R) = -2.5 \times \log \left[ a_1 \left( 1 + \left( \frac{R}{R_c} \right)^2 \right) \right]^\beta \quad (2)$$

with  $a_1 = 7.19 \times 10^{-8}$ ,  $R_c = 8.0''$ .

In Fig.5 we plot the new surface brightness profile that is now calibrated by the aperture photometry in the R-band from the catalogue of Prugniel and Heraudeau (1998). Equation 2 is an excellent representation of the brightness profile out to  $230''$  (or 31 kpc). Beyond, the model becomes a bit brighter than the galaxy, but this happens at a radius where shells already are visible and sphericity is obviously not longer a good approximation. The lower panel demonstrates that the model reproduces very well the aperture photometry.

This model (sometimes called the Modified Hubble Law) can be analytically deprojected to arrive at equation 3.

The deprojection gives for the luminosity density (unit  $L_\odot/\text{pc}^3$ )

$$j_0 = f \frac{a_1}{2r_c} \left[ 1 + \left( \frac{r}{r_c} \right)^2 \right]^{-\frac{3}{2}} \quad (3)$$

where the radii are now in pc and  $f = 2.505 \times 10^{10}$  is the factor that transforms surface brightness into solar luminosities per square pc. In addition, we apply a factor 1.19 to correct for foreground absorption in the R-band (see section 3.4). After spherical integration, one obtains for the cumulative mass

$$M(r) = 4\pi (M/L) f (a_1 / (2r_c)) \times \left[ -rr_c^2 / \sqrt{1 + (r/r_c)^2} + r_c^3 \ln \left( r/r_c + \sqrt{1 + (r/r_c)^2} \right) \right] \quad (4)$$

If we define 50 kpc to be a cut-off radius (large enough this specific choice does not affect much the half-light radius), the stellar half-mass radius is 8.5 kpc, which contains a mass of  $9.97 \times 10^{10} M_\odot$  adopting  $M/L_R = 4.2$  to be consistent with an age of 12 Gyr and a metallicity of  $[M/H] = -0.4$ . At this radius the MONDian mass expectation would be  $1.43 \times 10^{11} M_\odot$  (equation 6), corresponding to a dark matter fraction of 0.27, which can be compared with cosmological simulations.



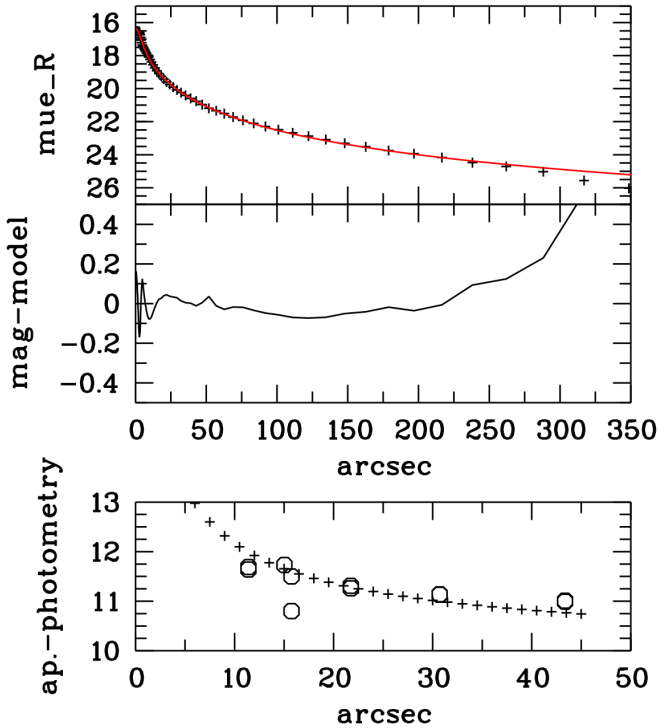


**FIGURE 5** Upper panel: Corrected surface brightness from Paper I and our new formula. Middle panel: Difference between measurements and our model. Lower panel: numerical aperture photometry of our model (crosses) is compared with the aperture photometry in the R-band of NGC 5812 in the catalogue of Prugniel and Heraudeau (1998). It shows the validity of our actual photometric calibration.

## 5.2 | Spherical Jeans models

The results from measuring the galaxy spectra can be seen in Fig.6 that shows the observed velocities and velocity dispersions together with dynamical models. In the following, we explain in detail what can be seen in Fig.6 .

The circles are measurements from Bertin et al. (1994), which are longslit data that in our figure have been folded into one radial coordinate. The scatter already at small radii is strikingly high. The red triangles are our measurements, the left panels display the values which resulted from the pPXF-fits with two moments, the right panels from the fits with four moments. There is a small systematic in that the 4-moment fits give slightly lower dispersions. We do not think that the values of the higher moments are interpretable and do not discuss them further. The main characteristics are the high central dispersion, the rapid decline and the large scatter at larger radii which is in line with the Bertin et al.-values.

The upper panels show baryonic Newtonian models, the lower panels their MONDian correspondence. Our models

uses the non-rotating spherical Jean-equation, as we did in previous papers. The Jeans-formalism was presented in many contributions, we refer the reader to Mamon and Łokas (2005) and Schuberth et al. (2010, 2012). We assign an  $M/L$ -ratio (R-band) to Eq.4 and calculate the projected velocity dispersions.

We first consider cases of isotropic models, which are shown in Fig.6 by the solid lines. The upper solid line represents an  $M/L_R$ -value of 5.8, motivated partly by the central population properties and partly by the wish to best reproduce the inner velocity dispersion values. The small central upturn is caused by a central black hole of  $10^9 M_\odot$  that we inserted to illustrate its negligible influence. The lower solid line represents  $M/L_R=4.2$ , motivated by the population gradient. It is obvious that these isotropic models are no good descriptions.

A suitable population mix would perhaps look more promising, but in the framework of spherical models, a better choice would be introducing a radial anisotropy. Pragmatically, we follow Hansen and Moore (2006) who found in merger simulations that the anisotropy is related to the logarithmic slope of the three-dimensional stellar mass distribution by

$$\beta = 1 - 1.15(1 + slope(r)/6). \quad (5)$$

From our photometric model,  $\beta$  would reach a constant radial anisotropy of +0.4 at about 5 kpc. A good approximation for this relation is the anisotropy profile considered by Mamon and Łokas (2005):  $\beta = 0.5(r/(r+r_a))$ ,  $r_a$  being a scale radius with some low value, we choose arbitrarily  $r_a = 450$  pc . Adopting this kind of anisotropy, we can conveniently apply the formalism given by Mamon and Łokas (2005).

This long-dashed lines in Fig.6 are calculated with this anisotropy and a global  $M/L_R$ -value of 4.2.

This model reproduces the initial decline of the velocity dispersion out to 3 kpc and indicates that within the assumption of sphericity, a radial anisotropy is needed. To show the extreme, the blue dashed-dotted line is a fully radial model (kernel "radial" of Mamon and Łokas 2005). This is of course unphysical. Moreover, the central velocity dispersion reaches about 2000 km/s, but the shape at larger radii is well reproduced. That such unphysical model seems to fit, may be an indication that spherical models are not adequate, but axisymmetric models would need the knowledge of the full velocity field and are beyond our scope.

The lower panels show the MONDian versions of the above models. We calculate the MONDian circular velocity with

$$v_M = \sqrt{v_N^2(r)/2 + \sqrt{v_N^4(r)/4 + v_N^2(r)a_0r}}, \quad (6)$$

where we adopt  $a_0 = 1.35 \times 10^{-8} cm/sec^2$  (Famaey, Gentile, Bruneton, & Zhao, 2007) and  $v_N$  is the Newtonian circular velocity.

The MONDian version with  $M/L_R=5.8$  would be far off from the observations, so we do not give it. It is also obvious



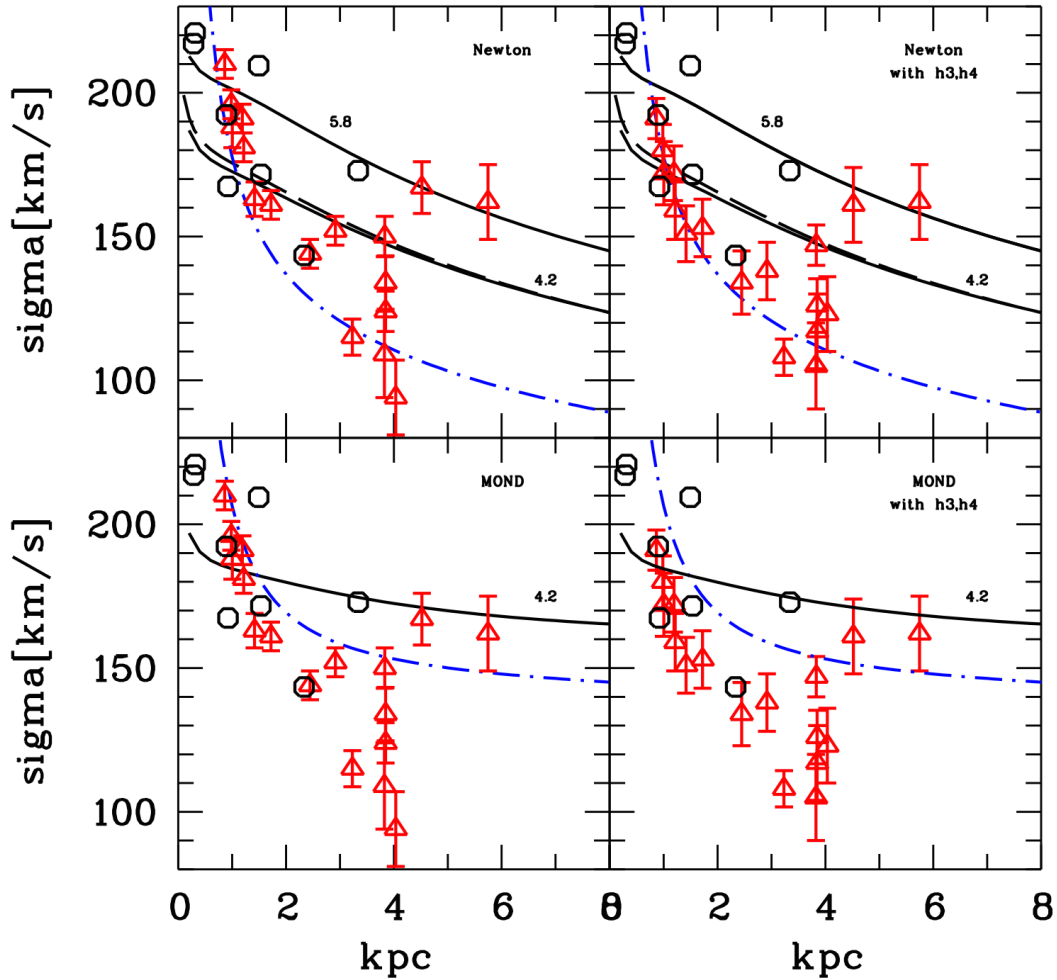


**FIGURE 6** Velocity dispersions of the galaxy light and various spherical Jeans-models of which none is satisfactory. The circles mark long-slit measurements from Bertin et al. (1994). The triangles are our measurements. **Upper panels:** The upper panels show baryonic Newtonian models. The left panel shows pPXF results, fitting two moments, the right panel fitting four moments. The solid lines are isotropic models with stellar  $M/L_R$ -values of 5.8 (upper line) and 4.2 (lower line). They do not reproduce the measurements well. The dashed line (in both panels) is a model with  $M/L_R=4.2$  and the radial anisotropy of Hansen and Moore (2006) (see text) and may represent the inner dispersion profile, but fails at larger radii. The blue dashed-dotted line (in both upper panels) is a fully radial model, which seems to fit most of the measurements, but is unphysical. Lower panels: The lower panels show the corresponding MONDian models for an  $M/L_R$ -value of 4.2 (there is no point for showing 5.8). They do not fit. See text for more remarks.

that this kind of MOND models is not satisfactory. By fine-tuning  $M/L$ , anisotropy and MONDian/not-MONDian, one may find a more or less good representation for the inner parts. The wide scatter of velocity dispersion at a given radius rather suggests that a purely spherical Jeans model is not an adequate description. At any case, there is no evidence for a significant spherical halo of dark matter. In an axisymmetric model, the MOND force may exist perpendicular to the line-of-sight.

However, a dark matter halo is not visible under sphericity. The question, whether spherical Jeans-models are adequate

at all, is difficult to answer. In an ideal spherical "Jeans-world" there is a unique relation between velocity dispersion and radius. A significant scatter could indicate that dynamical equilibrium is not reached and the MONDian force would be hidden.

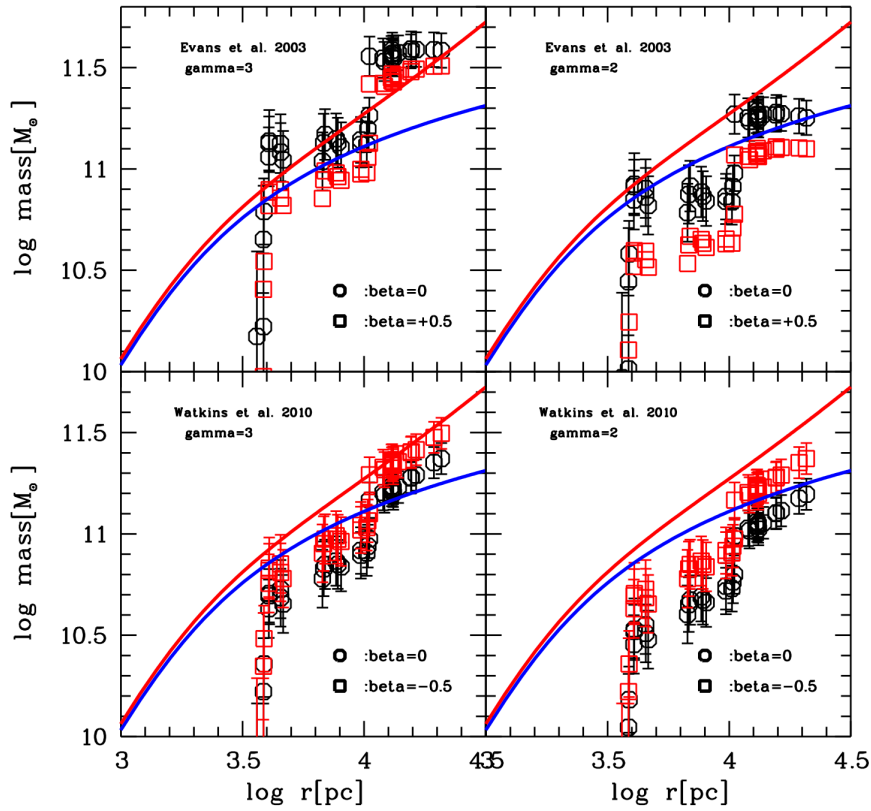


**FIGURE 7** Two mass estimators with different parameters, applied consecutively. Sensibly, only the outer points carry sensible mass information. Upper panels: the estimator of Evans et al. (2003). Lower panels: the estimator of Watkins et al. (2010). Left and right panels: the tracer’s density power law profile with  $\gamma=3$  and  $\gamma=2$ , respectively. Upper panels: Black symbols stand for isotropy, red for radial anisotropy with  $\beta=+0.5$ . Lower panels: black symbols denote isotropy and red symbols tangential anisotropy with  $\beta=-0.5$ . The black solid lines denote purely baryonic mass profiles for an  $M/L_R$  of 4.2 for consistency with Fig.6 . The red solid lines are MOND profiles. Only for a very flat tracer density profile, the data are not compatible with MOND. In this case, it would be a dark matter free galaxy.

## 6 | MASS ESTIMATORS

For larger radii, we use the GC velocities to further constrain the mass profile. Given the low number of velocities, we do not attempt any Jeans modelling, but apply ”tracer mass estimators”. These mass estimators have a long history (Bahcall & Tremaine, 1981; Heisler, Tremaine, & Bahcall, 1985; White, 1981) with the motivation of using only projected radii and radial velocities for a reasonable mass estimation. Here we use the estimators proposed by Evans et al. (2003) and Watkins et al. (2010). These mass estimators have the form

$$\frac{C}{GN} \times \sum v_{LOS,i}^2 R_i \quad (7)$$

with  $G$  the constant of gravitation,  $N$  the number of tracers, and  $C = C(\alpha, \beta, \gamma)$  being a constant that includes properties of the potential and the tracer population. For further physical reasoning and brevity, we refer to the original papers. The parameters are the three-dimensional tracer’s density profile described by a power-law exponent  $\gamma$  and the orbital anisotropy  $\beta$ . Furthermore,  $\alpha$  is the exponent of a power-law potential. We assume an isothermal potential, which is supported also for elliptical galaxies, so  $\alpha = 0$ . We calculate the uncertainties of the sum in equation 7 using the individual velocity uncertainties. However, a major contribution to the absolute mass uncertainties come from systematics (deviation from virial equilibrium, distance, properties of the tracer populations). Therefore, we

show in the four panels of Fig.7 the relation between the stellar model (blue line) and its MONDian correspondence (red line) and the masses derived with the mass estimators for various parameters.  $M/L_R=4.2$  has been adopted to be consistent with the Jeans-analysis.

The upper two panels employ the constants given by Evans et al. (2003), the lower two panels those by Watkins et al. (2010). We apply the mass estimator consecutively, which means for the about first 20 velocities the mass profile is of course not really constrained. We vary  $\gamma$ , the tracer profile, and the anisotropy parameter. The left panel has  $\gamma = 3$ , which matches the galaxy light, and the right panel  $\gamma = 2$ .  $\gamma = 3$  may describe the inner GC population well whose distribution should be similar to the galaxy light. Values a bit less and around  $\gamma = 2$  are typical for the outer and more metal-poor GCs which are donated through the infall of dwarf galaxies, which in our case of a isolated elliptical will not be many and is a reason for the paucity of the cluster system.  $\gamma$  is not well constrained (see Fig.9 of Lane et al. 2013), but the above values embrace the systematic uncertainty.

In all panels, the black symbols represent isotropic models, and the red symbols represent anisotropic models.

The red symbols in the upper panel represent radial anisotropies of  $\beta = +0.5$ , the red symbols in the lower panels represent tangential anisotropy of  $\beta=-0.5$ .

The most general statement is that the GCs do not indicate a significant dark matter halo beyond the MOND expectation. MOND is supported with a steep number density profile, rather independent from the anisotropy. A radial anisotropy together with a flatter profile would also be consistent with MOND. The non-Gaussian velocity distribution speaks for a moderate radial anisotropy, which reflects the anisotropy of the stellar population. A flat profile together with a tangential anisotropy would indicate a galaxy free of dark matter.

An interesting observation is the jump in the mass profile at 10 kpc. One could classify this as a statistical feature without much meaning, but parallel one notes that beyond 10 kpc, only blue, metal-poor GCs appear which suggests a flatter density profile. That means that until 10 kpc,  $\gamma$  would be close to 3 and beyond,  $\gamma$  would be closer to 2. That would be consistent with the stellar model at 10 kpc and would at least soften the jump.

## 7 | DISCUSSION

Our aim with the following discussion is to place our results within the context of the current literature wisdom.

### 7.1 | Comparison with simulated galaxies

Galaxies like NGC5812 or NGC7507 are so far not identified in cosmological simulations. Older work of Niemi, Heinämäki, Nurmi, and Saar (2010) does not find a large difference regarding the dark matter content between isolated and non-isolated elliptical galaxies. The recent project Illustris-TNG can perhaps be regarded as the most complete simulations available. Fig.6 of Lovell et al. (2018) shall be our reference. Galaxies with stellar masses like NGC 5812 show a median dark matter fraction of 0.7 within one half-mass radius which is not compatible with the present state of data, which permits at most the MONDian correspondence of 0.27. One might object that NGC5812 is an elliptical galaxy still in the making and may be better compared with galaxies of higher redshift, but that is beyond the scope of our paper.

### 7.2 | Dark matter characteristics and the Baryonic Tully Fisher relation

It is now interesting to put these results into the general context of dark matter in early-type galaxies. What is the present understanding of the relation between dark and luminous matter? Much work during the last decades has shown that there is a close relation between the baryonic mass and the dark mass of disk galaxies.

The well-defined "baryonic Tully-Fisher relation" (BTFR) for disk galaxies has been shown various times (McGaugh, 2005, 2012; Stark, McGaugh, & Swaters, 2009; Trachternach, de Blok, McGaugh, van der Hulst, & Dettmar, 2009). The literature figures should be updated by including six dwarf galaxies from Kurapati, Chengalur, Pustilnik, and Kamphuis (2018). These dwarfs are found in the Lynx-Cancer void, a region of very low galaxy density and (within the world of LCDM) also of low dark matter density. It is remarkable how well these galaxies fit to the relation given by McGaugh (2005). It is hard to imagine that such a tight relation for disk galaxies of such different mass in such different environments shall be the result of galaxy formation in dark matter halos.

The dynamical properties of disk galaxies appear *as if* the Newtonian law of gravity would be modified according to Milgrom's prescription (J. Bekenstein & Milgrom, 1984; Milgrom, 1983a, 1983b). Understanding the parent theory of MOND as a new law of gravitation or as modified inertia, of which MOND is the non-relativistic limit, has inspired a wealth of theoretical effort (for a review see Famaey and McGaugh 2012; see also sections 1.5.8 and 1.5.9 in Amendola et al. 2016).

Interesting thoughts developed recently within the framework of a thermodynamical interpretation of gravity. Starting with J. D. Bekenstein (1973) and Hawking (1975), who introduced entropy and temperature in black hole physics, Gibbons

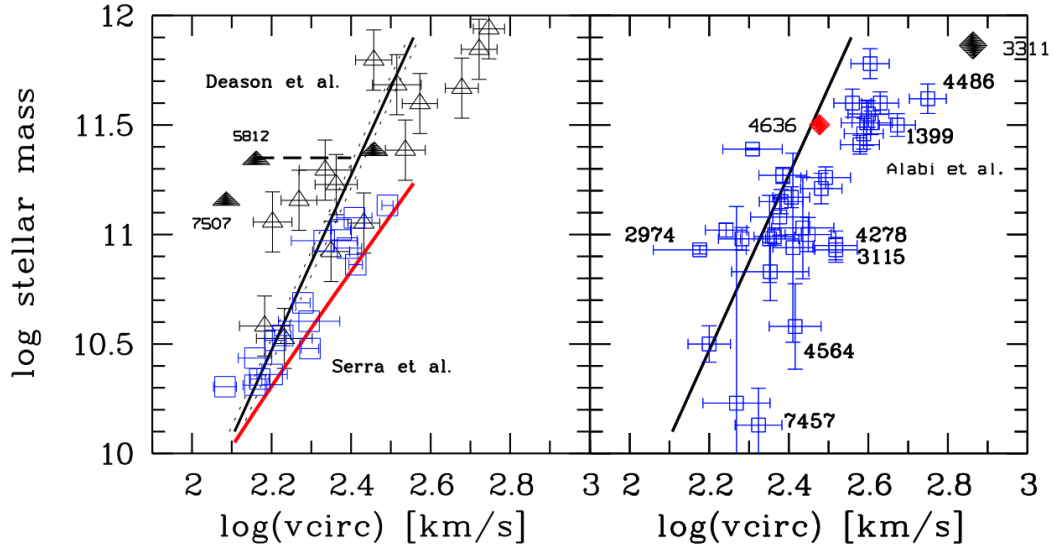


**FIGURE 8** This figure demonstrates in a compact manner, what it currently known about masses of early-type galaxies at large radii. It displays the total baryonic masses within five effective radii vs. the circular velocity at this radius for various samples. The two panels are identical for better readability. The solid lines in both panels indicate the BTFR for disk galaxies from McGaugh (2005), including the  $1\text{-}\sigma$ -scatter as the dashed lines. Left panel: the triangles denote the sample of Deason et al. (2012), the squares the sample of Serra et al. (2016). The red solid line is the BTFR that results from cosmological simulations (Sales et al., 2017). The uncertainties have been calculated by error propagation using the literature information. The intrinsic scatter of the BTFR may be much smaller than the scatter appearing in the graph. Two isolated elliptical galaxies appear with their NGC numbers without uncertainties, because there may be unknown systematics (this paper and Lane et al. 2013). The bar right of NGC 5812 indicates the range which is compatible with the data. Right panel: blue squares denote the SLUGGs survey (Alabi et al., 2017). The most deviant galaxies are indicated by their NGC numbers. The red diamond is NGC 4636 to which we assign particular weight for its large number of tracers (Schuberth et al., 2012). The bright deviant galaxies are central cluster galaxies. An additional central cluster galaxy, NGC 3311, is indicated (Hilker et al., 2018).

and Hawking (1977) generalized these concepts for cosmological event horizons. Jacobson (1995) showed how the Einstein equation can be perceived as a thermodynamical equation of state. Strominger and Vafa (1996) demonstrated the microscopic origin of the Bekenstein black hole entropy. Space-time and gravity may emerge from a microscopic degrees of freedom, e.g. Padmanabhan (2015, 2018). Verlinde (2011) proposed to describe gravity as an entropic force and Verlinde (2017) showed how the MONDian phenomenology may be derived from this conception in a de Sitter-Universe. Hossenfelder (2017) provided a covariant version of Verlinde’s concept and Hossenfelder and Mistele (2018) derived a spherically symmetric non-relativistic limit, which, although physically different, is the MOND formula in practice.

However, theoretical ideas around MOND are evolving, see the recent work of Milgrom (2023) and Skordis and Złośnik (2021).

If these new physical concepts are valid, every galaxy *must* show a MONDian appearance. In particular, elliptical galaxies must fall on the same BTFR as disk galaxies. Apparently, this was not the case in the samples of Gerhard, Kronawitter, Saglia, and Bender (2001) and Magorrian and Ballantyne (2001), but these studies did not reach out to large radii, where dark matter or mass discrepancies leave their imprints. On the other hand, some elliptical galaxies have been found, which are well consistent with MOND and therefore fall onto the BTFR for spiral galaxies (Milgrom, 2012; Schuberth et al., 2012; Weijmans et al., 2008).

There is a reason for the fact that the MONDian phenomenology among ellipticals is not so clear-cut as for spirals. Spiral galaxies permit a relatively easy access to their dynamics by offering the convenience of a disk with more or less circular orbits. This disk symmetry is generally missing in ellipticals and consequently, mass determinations of elliptical galaxies can be rather uncertain, even when the kinematical data are good or even excellent. Among the dynamically best

known ellipticals are NGC 3379 and NGC 4494. In spite of the detailed dynamical knowledge, theoretical models which are consistent with the data span a large variety of dark matter properties (de Lorenzi et al., 2009; Morganti, Gerhard, Coccato, Martinez-Valpuesta, & Arnaboldi, 2013), including a MONDian behaviour.

Therefore it is interesting to overcome the individual uncertainty by considering a larger sample of elliptical galaxies with kinematic data reaching out to large radii which has been treated homogeneously. There are now several samples of interest. These appear in Fig.8 in the left and the right panel. The abscissae are the log of the circular velocity at 5 effective radii, the ordinates are the total baryonic mass (stars+gas) as indicated in the samples. The black solid lines in both panels denote the BTFR for disk galaxies of (McGaugh, 2005)  $M_{baryonic} = 50 \times v_f^4$  where  $M_{baryonic}$  is the baryonic (stars+gas) mass of the galaxy and  $v_f$  the rotational velocity on the flat part of the rotation curve. In the left panel, the uncertainty is indicated by the two dotted lines. The red line represents the mean locus of the BTFR that emerges from cosmological simulations (Sales et al., 2017). The triangles in the left panel denote the galaxy sample of Deason et al. (2012) who homogenised the available kinematic data from the literature and derived masses for 15 ellipticals applying mass indicators based on tracer populations. The baryonic masses have been calculated by using the mass-to-light ratios of Cappellari et al. (2011). The uncertainties have been adopted from the sample descriptions. They may be even somewhat underestimated, given the fact that the basic distance uncertainty of an individual galaxy is of the order 15%-20%. The observed scatter may be largely explained by these uncertainties. Then there is the interesting sample of Serra et al. (2016) early-type galaxies with HI-disks who measured the rotation curves in 16 galaxies (blue squares in Fig.8, left panel). Because the inclination of the HI-disk can be determined with high confidence, the calculated masses may count as more precise than those derived from tracers like GCs and planetary nebulae. They point out the strong coupling between dark and luminous matter by the relation

$$V_{circular}(5R_e) = 1.33 \times \sigma_e \quad (8)$$

where  $R_e$  is the effective radius and  $\sigma_e$  the LOV velocity dispersion within one  $R_e$ . This relation varies the well-known relation  $V_{circular} = \sqrt{3}\sigma_{LOS}$  for an isothermal, isotropic system. It is obvious that they rediscovered MOND for their sample. These two samples are well consistent with the BTFR of disk galaxies, except for our isolated ellipticals and some massive galaxies that in fact are prominent central galaxies.

Another even larger sample of 34 ellipticals has been provided by the SLUGGS survey (Alabi et al., 2017) that uses GC radial velocities for mass determinations at larger radii (blue symbols in the right panel of Fig.8). The total number of GC

velocities is impressively 2500 and some galaxies have several hundred GCs to be used as tracers for the potential. The mean locus of the SLUGGS-sample is clearly displaced from the spiral BTFR. The most deviating galaxies are indicated and commented on in the next section. In many cases there are reasons to doubt the high masses. The red diamond is NGC 4636, whose location is based on the velocities of 460 globular clusters (Schuberth et al., 2012) and therefore has particular weight.

## 7.3 | Galaxies deviating from the BTFR

The indications for a general MONDian phenomenology are so strong that the deviators from the MONDian relation are at least as interesting as those agreeing. It is of course beyond the scope of our paper to discuss in detail every galaxy that appears deviating from the BTFR. On the long term this will be necessary, but here we restrict ourselves to a few remarks that suggest that the presented masses still need confirmation.

### 7.3.1 | Dark matter dominated galaxies

If the new concepts of gravity are viable, there is no reason to expect dark matter at all, meaning that it is potentially possible to falsify this proposed nature of gravity just by a quick look at Fig.8, where there are many examples deviating from the BTFR. Therefore the question is important, whether the deviations mean solid and irrefutable facts or whether these galaxy masses are due to incomplete data and/or systematic effects that are not yet understood. The obviously deviating galaxies in the Deason et al. sample survey are NGC 1399 and M87, both central galaxies of a cluster or subcluster, respectively. It is common wisdom (perhaps erroneous) that MOND does not account for all dark matter in galaxy clusters (e.g. Angus et al. 2008), and therefore central galaxies are particularly expected to host huge dark matter halos. NGC1399 is a rather mild example (Richtler et al., 2008). NGC 3311 as the central galaxy of the HydraI cluster with its strongly rising velocity dispersion is a stronger example of a galaxy that has been putatively associated with a large cored halo (Richtler et al., 2011). However, recent work has shown that the rising velocity dispersion may rather be the result of mixing of different tracer populations in a very inhomogeneous velocity field (Hilker et al., 2018). It cannot be shown on the one hand that NGC 3311 is MONDian, but on the other hand there is no "clean Jeans-world" and no spherical symmetry, so mass determinations based on Jeans-models are doubtful.

Other galaxies with dark matter content much higher than allowed by the BTFR are NGC 7457, 4564, 3115, 4278. NGC 4278 is also a galaxy in the Serra et al. sample and there fits well to the BTFR. NGC 7457 is the faintest galaxy in the entire sample.

The data quality plays a role and also our present sample certainly leaves room for improvement.

### 7.3.2 | Dark matter poor galaxies

In the sample of Gerhard et al. (2001), the isolated elliptical NGC 7507 was the most dark matter dominated galaxy. In strong contrast, Lane et al. (2015); Salinas et al. (2012) using much more complete data, were able to produce models of NGC 7507 that did not require any dark matter. Another isolated elliptical with contradicting dark matter content is NGC 4697, whose possible dark matter halo was labelled "inconspicuous" by Méndez, Teodorescu, Kudritzki, and Burkert (2009), using the kinematics of over 500 PNe. This object appeared as one of the most dark matter dominated galaxies in Alabi et al. (2016) and still containing a lot of dark matter in Alabi et al. (2017) on the basis of 20 GC velocities. Another dark matter-poor galaxy is NGC 2974, which is also in the Serra et al. sample, where it fits well to the BTFR. See also Weijmans et al. (2008) who describe this galaxy as being MONDian.

NGC 5812 may be another example where a low number of tracers together with a system still approaching an equilibrium does not permit to derive a trustworthy mass. Complete velocity fields of the outer regions of early-type galaxies can be observed with large field IFUs, and may help to understand better their dynamics.

### 7.4 | X-ray masses of isolated ellipticals

The data from Fig.8 are of stellar dynamical origin. However, many early-type galaxies are X-ray bright, and therefore under the assumption of hydrostatical equilibrium, provide the possibility to derive masses, among them isolated ellipticals. We do not aim at completeness, but refer the reader to some particular cases, where X-ray analyses indeed indicate the location of galaxies on the BTFR.

That the two isolated elliptical galaxies NGC 720 and NGC 1521 obey the MONDian prediction has been shown by Milgrom (2012), (non-MONDian analyses and X-ray data from Humphrey, Buote, Canizares, Fabian, and Miller 2011 and Humphrey, Buote, O'Sullivan, and Ponman 2012). The mass modelling of NGC 7796 (Richtler et al., 2015) (X-ray data from O'Sullivan, Sanderson, and Ponman 2007) showed at least consistency with the MONDian prediction. More X-ray masses of early-type galaxies in the MONDian context has been listed by (Lelli et al., 2017). Their thorough study of the "Radial Acceleration Relation of Galaxies" includes 240 galaxies of various types, among them also 25 early-type galaxies (their Table 3), of which 16 belong to the kinematic sample of Serra et al. (2016) and entered already Fig.8. Among the remaining X-ray based objects is NGC 6482 remarkable as a further

isolated elliptical on the BTFR. All these data let the "pure baryonic" galaxy NGC 7507 so far appear as a not-understood exception.

### 7.5 | Bayesian fits to rotation curves

The MOND phenomenology appears with a different flavour as a "universal acceleration scale" in disk galaxies (Lelli et al., 2017). This scale then should also exist in elliptical galaxies. An alternative approach to dynamics of elliptical galaxies has been to fit "rotation curves", by means of bayesian techniques, using as input data the light profiles and projected velocity dispersions and fitting a sequence of parameters with certain priors and assumption, including mass-to-light ratios and the anisotropy. The results so far are controversial. Chae, Bernardi, Domínguez Sánchez, and Sheth (2020) found indeed a universality of the acceleration scale. However, the Bayesian techniques has been criticised by Li, Lelli, McGaugh, Schombert, and Chae (2021) who cautioned the use of degenerated parameters and demonstrated that  $G$ , the constant of gravitation, may turn out different from galaxy to galaxy.

Recently, Chan, Desai, and Del Popolo (2022) found for a sample of MaNGA galaxies the acceleration scale by roughly a factor 1.5 higher than that for spiral galaxies. They boldly conclude that there is no universal acceleration among galaxies and take that as a falsification for MOND. However, they found for most of their round galaxies a significant tangential anisotropy. To our knowledge, such an anisotropy has never been observed elsewhere in the literature of the dynamics of elliptical galaxies, so its reality as a characteristic for elliptical galaxies may be doubted. Because this value appears as  $-2 \times \beta$  in the Jeans equation for the galaxy mass, it may well account for the difference to the acceleration scales of spirals. Therefore we suspect that this may be an example for Li and al.'s precaution.

### 7.6 | Concluding remarks

These examples show that the present data do not permit a final convincing conclusion whether or not early-type galaxies fall onto the BTRF of spiral galaxies. This seems to be a sample property, some samples agreeing with the MONDian prediction, others not. However, there are indications that data quality and completeness play an important role. Central galaxies seem to be clearly not MONDian, but NGC 3311 may be an example for the possibility that tracer properties can fake a huge dark halo that in reality does not exist. At the isolated ellipticals end, NGC 7507 stands still as a candidate galaxy without dark matter. Perhaps the observation of a full velocity field will bring clarity.

## 8 | SUMMARY AND CONCLUSIONS

We investigated the dynamics of the isolated elliptical NGC5812 with a database of spectroscopic Gemini/GMOS masks, using the galaxy light and globular clusters as dynamical tracers.

We could identify 24 globular clusters at galactocentric distances between 10 kpc and 23 kpc (the adopted distance is 28 Mpc) and applied the tracer mass estimators of Evans et al. (2003) and Watkins et al. (2010). As for the galaxy light, we measured velocities and velocity dispersion values out to a distance of 6 kpc. We revised the photometric model from previous works. NGC 5812 has a spherical appearance, but a subtraction of a spherical model leaves significant residuals, so one may expect the spherical symmetry to be violated as previous long slit spectroscopy already suggested. While the velocity dispersion profile seems to be well defined out to 2 kpc, one finds a large scatter at larger radii. Therefore we refrained from stacking spectra at different position angles. The central spectra show an old, metal-rich population showing a metallicity gradient. We constructed several Jeans-model mass profiles, which assume spherical symmetry. We need a stellar mass-to-light ratio of  $M/L_R = 4.0$  in combination with a slight radial bias for reproducing the central velocity dispersion profile. Isotropic models do not work well. This might correspond to the velocity distribution of globular clusters that is not purely Gaussian, but exhibits a significant kurtosis. We then can compare the baryonic mass with the dynamical mass, which ideally should be manifest in the kinematics of the globular clusters. Our mass estimators assume spherical symmetry (which also means a smooth population of phase space) and virial equilibrium. We find consistency with the MONDian expectation, but purely baryonic models are not excluded. However, the data seem to exclude a massive dark halo.

One of the globular clusters is extraordinarily bright  $M_R \approx -12.2$ . We estimate its mass to be  $1.6 \times 10^7 M_\odot$ . We also could measure a radial velocity for the dwarf companion with a tidal tail which indicates a very elongated orbit as expected.

The case for a MONDian phenomenology also among early-type galaxies has become so strong (e.g. Lelli et al. 2017) that deviations from a MONDian behaviour appear more interesting than agreements, because there is an astrophysical problem to solve. In our previous work, NGC 7507 already appeared as an dark matter-free galaxy. We embed the results for NGC 5812 in the present literature for dark matter in early-type galaxies, using the galaxy samples of Deason et al. (2012) and Serra et al. (2016), which strongly argue for the fact that elliptical galaxies fall onto the same baryonic Tully-Fisher relation as spiral galaxies, The sample of ellipticals of Alabi et al. (2017) (the SLUGGs-survey) does not show that so clearly.

The (unavoidable) deficiency of our analysis is beside the relative small number of probes the application of mass estimators that assume spherical symmetry and dynamical equilibrium. It may be that the velocity dispersion field does not contain the full kinematical information and that a full velocity map is necessary to reliably derive a mass profile together with more insight in its internal structure.

## ACKNOWLEDGEMENTS

TR acknowledges financial support from FONDECYT project Nr. 1100620, and from the BASAL Centro de Astrofísica y Tecnologías Afines (CATA) PFB-06/2007. TR thanks ESO for several invitations as science visitor, where a major part of this work has been accomplished. TR thanks Mike Fellhauer for a class on tidal tails. We are thankful to Bryan Miller for essential help with the GMOS data reductions.

## REFERENCES

- Alabi, A. B., Forbes, D. A., Romanowsky, A. J. et al. (2016, August), *MNRAS*, *460*, 3838-3860. doi:
- Alabi, A. B., Forbes, D. A., Romanowsky, A. J. et al. (2017, July), *MNRAS*, *468*, 3949-3964. doi:
- Amendola, L., Appleby, S., Avgoustidis, A. et al. (2016, June), *ArXiv e-prints*.
- Angus, G. W., Famaey, B., & Buote, D. A. (2008, July), *MNRAS*, *387*(4), 1470-1480. doi:
- Bahcall, J. N., & Tremaine, S. (1981, March), *ApJ*, *244*, 805-819. doi:
- Bekenstein, J., & Milgrom, M. (1984, November), *ApJ*, *286*, 7-14. doi:
- Bekenstein, J. D. (1973, April), *Phys. Rev. D*, *7*, 2333-2346. doi:
- Bertin, G., Bertola, F., Buson, L. M. et al. (1994, December), *A&A*, *292*, 381-391.
- Bertone, G. (2010, November), *Nature*, *468*, 389-393. doi:
- Bertone, G., & Hooper, D. (2018, October), *Reviews of Modern Physics*, *90*(4), 045002. doi:
- Bertone, G., Hooper, D., & Silk, J. (2005, January), *Phys. Rep.*, *405*, 279-390. doi:
- Bertone, G., & Tait, T. M. P. (2018, October), *Nature*, *562*(7725), 51-56. doi:
- Binney, J., & Tremaine, S. 2008, *Galactic Dynamics: Second Edition*.
- Bressan, A., Marigo, P., Girardi, L., Salasnich, B., Dal Cero, C., Rubele, S., & Nanni, A. (2012, November), *MNRAS*, *427*, 127-145. doi:
- Cappellari, M. (2017, April), *MNRAS*, *466*(1), 798-811. doi:
- Cappellari, M., & Emsellem, E. (2004, February), *PASP*, *116*(816), 138-147. doi:
- Cappellari, M., Emsellem, E., Krajnović, D. et al. (2011, September), *MNRAS*, *416*, 1680-1696. doi:
- Chae, K.-H., Bernardi, M., Domínguez Sánchez, H., & Sheth, R. K. (2020, November), *ApJ*, *903*(2), L31. doi:
- Chan, M. H., Desai, S., & Del Popolo, A. (2022, May), *arXiv e-prints*, arXiv:2205.07515.



- Cherenkov Telescope Array Consortium, Acharya, B. S., Agudo, I. et al. 2019, Science with the Cherenkov Telescope Array. doi:
- de Lorenzi, F., Gerhard, O., Coccato, L. et al. (2009, May), *MNRAS*, 395, 76-96. doi:
- Deason, A. J., Belokurov, V., Evans, N. W., & McCarthy, I. G. (2012, March), *ApJ*, 748, 2. doi:
- Di Valentino, E., Melchiorri, A., & Silk, J. (2020, February), *Nature Astronomy*, 4, 196-203. doi:
- Dirsch, B., Richtler, T., Geisler, D., Forte, J. C., Bassino, L. P., & Gieren, W. P. (2003, April), *AJ*, 125, 1908-1925. doi:
- Evans, N. W., Wilkinson, M. I., Perrett, K. M., & Bridges, T. J. (2003, February), *ApJ*, 583, 752-757. doi:
- Fahrión, K., Georgiev, I., Hilker, M. et al. (2019, May), *A&A*, 625, A50. doi:
- Famaey, B., Gentile, G., Bruneton, J.-P., & Zhao, H. (2007, March), *Phys. Rev. D*, 75(6), 063002. doi:
- Famaey, B., & McGaugh, S. (2013, October), *ArXiv e-prints*.
- Famaey, B., & McGaugh, S. S. (2012, September), *Living Reviews in Relativity*, 15(1), 10. doi:
- Gerhard, O., Kronawitter, A., Saglia, R. P., & Bender, R. (2001, April), *AJ*, 121, 1936-1951. doi:
- Gibbons, G. W., & Hawking, S. W. (1977, May), *Phys. Rev. D*, 15, 2738-2751. doi:
- Hansen, S. H., & Moore, B. (2006, March), *New A*, 11, 333-338. doi:
- Harris, H. C., & Canterna, R. (1977, October), *AJ*, 82, 798-804. doi:
- Hawking, S. W. (1975, August), *Communications in Mathematical Physics*, 43, 199-220. doi:
- Heinesen, A., & Buchert, T. (2020, August), *Classical and Quantum Gravity*, 37(16), 164001. doi:
- Heisler, J., Tremaine, S., & Bahcall, J. N. (1985, November), *ApJ*, 298, 8-17. doi:
- Hilker, M., Richtler, T., Barbosa, C. E., Arnaboldi, M., Coccato, L., & Mendes de Oliveira, C. (2018, November), *A&A*, 619, A70. doi:
- Hossfelder, S. (2017, June), *Phys. Rev. D*, 95(12), 124018. doi:
- Hossfelder, S., & Mistele, T. (2018, January), *International Journal of Modern Physics D*, 27(14), 1847010. doi:
- Humphrey, P. J., Buote, D. A., Canizares, C. R., Fabian, A. C., & Miller, J. M. (2011, March), *ApJ*, 729(1), 53. doi:
- Humphrey, P. J., Buote, D. A., O'Sullivan, E., & Ponman, T. J. (2012, August), *ApJ*, 755(2), 166. doi:
- Jacobson, T. (1995, August), *Physical Review Letters*, 75, 1260-1263. doi:
- Kroupa, P. (2015, February), *Canadian Journal of Physics*, 93, 169-202. doi:
- Kurapati, S., Chengalur, J. N., Pustilnik, S., & Kamphuis, P. (2018, September), *MNRAS*, 479, 228-239. doi:
- Lane, R. R., Salinas, R., & Richtler, T. (2013, January), *A&A*, 549, A148. doi:
- Lane, R. R., Salinas, R., & Richtler, T. (2015, February), *A&A*, 574, A93. doi:
- Lelli, F., McGaugh, S. S., Schombert, J. M., Desmond, H., & Katz, H. (2019, April), *MNRAS*, 484(3), 3267-3278. doi:
- Lelli, F., McGaugh, S. S., Schombert, J. M., & Pawlowski, M. S. (2017, February), *ApJ*, 836(2), 152. doi:
- Li, P., Lelli, F., McGaugh, S., Schombert, J., & Chae, K.-H. (2021, February), *A&A*, 646, L13. doi:
- Lovell, M. R., Pillepich, A., Genel, S. et al. (2018, December), *MNRAS*, 481(2), 1950-1975. doi:
- Magorrian, J., & Ballantyne, D. (2001, April), *MNRAS*, 322, 702-714. doi:
- Mamon, G. A., & Łokas, E. L. (2005, November), *MNRAS*, 363, 705-722. doi:
- McGaugh, S. S. (2005, October), *ApJ*, 632, 859-871. doi:
- McGaugh, S. S. (2012, February), *AJ*, 143, 40. doi:
- McGaugh, S. S., Lelli, F., & Schombert, J. M. (2016, November), *Physical Review Letters*, 117(20), 201101. doi:
- Méndez, R. H., Teodorescu, A. M., Kudritzki, R.-P., & Burkert, A. (2009, January), *ApJ*, 691, 228-240. doi:
- Milgrom, M. (1983a, July), *ApJ*, 270, 365-370. doi:
- Milgrom, M. (1983b, July), *ApJ*, 270, 371-383. doi:
- Milgrom, M. (1983c, July), *ApJ*, 270, 384-389. doi:
- Milgrom, M. (2012, September), *Physical Review Letters*, 109(13), 131101. doi:
- Milgrom, M. (2023, September), *Phys. Rev. D*, 108(6), 063009. doi:
- Morganti, L., Gerhard, O., Coccato, L., Martínez-Valpuesta, I., & Arnaboldi, M. (2013, June), *MNRAS*, 431, 3570-3588. doi:
- Niemi, S.-M., Heinämäki, P., Nurmi, P., & Saar, E. (2010, June), *MNRAS*, 405, 477-493. doi:
- Ostriker, J. P., & Steinhardt, P. J. (1995, October), *Nature*, 377, 600-602. doi:
- O'Sullivan, E., Sanderson, A. J. R., & Ponman, T. J. (2007, October), *MNRAS*, 380(4), 1409-1421. doi:
- Padmanabhan, T. (2015, February), *Modern Physics Letters A*, 30, 1540007. doi:
- Padmanabhan, T. (2018, January), *International Journal of Modern Physics D*, 27(14), 1846004. doi:
- Planck Collaboration, Ade, P. A. R., Aghanim, N. et al. (2014, November), *A&A*, 571, A16. doi:
- Pointecouteau, E., & Silk, J. (2005, December), *MNRAS*, 364, 654-658. doi:
- Prugniel, P., & Heraudeau, P. (1998, March), *A&AS*, 128, 299-308. doi:
- Pryor, C., & Meylan, G. (1993, January), Velocity Dispersions for Galactic Globular Clusters. In S. G. Djorgovski & G. Meylan (Eds.), *Structure and Dynamics of Globular Clusters Vol. 50*, p. 357.
- Richtler, T., Dirsch, B., Gebhardt, K. et al. (2004, April), *AJ*, 127, 2094-2113. doi:
- Richtler, T., Salinas, R., Lane, R. R., Hilker, M., & Schirmer, M. (2015, February), *A&A*, 574, A21. doi:
- Richtler, T., Salinas, R., Misgeld, I. et al. (2011, July), *A&A*, 531, A119+. doi:
- Richtler, T., Schuberth, Y., Hilker, M., Dirsch, B., Bassino, L., & Romanowsky, A. J. (2008, February), *A&A*, 478, L23-L26. doi:
- Romanowsky, A. J., Douglas, N. G., Arnaboldi, M. et al. (2003, September), *Science*, 301, 1696-1698. doi:
- Sales, L. V., Navarro, J. F., Oman, K. et al. (2017, January), *MNRAS*, 464, 2419-2428. doi:
- Salinas, R., Richtler, T., Bassino, L. P., Romanowsky, A. J., & Schuberth, Y. (2012, February), *A&A*, 538, A87. doi:
- Sanders, R. H. (2003, July), *MNRAS*, 342, 901-908. doi:
- Schuberth, Y., Richtler, T., Dirsch, B., Hilker, M., Larsen, S. S., Kissler-Patig, M., & Mebold, U. (2006, November), *A&A*, 459, 391-406. doi:
- Schuberth, Y., Richtler, T., Hilker, M., Dirsch, B., Bassino, L. P., Romanowsky, A. J., & Infante, L. (2010, April), *A&A*, 513, A52+. doi:
- Schuberth, Y., Richtler, T., Hilker, M., Salinas, R., Dirsch, B., & Larsen, S. S. (2012, August), *A&A*, 544, A115. doi:
- Serra, P., Oosterloo, T., Cappellari, M., den Heijer, M., & Józsa, G. I. G. (2016, August), *MNRAS*, 460, 1382-1389. doi:
- Silverwood, H., Weniger, C., Scott, P., & Bertone, G. (2015, March), *J. Cosmology Astropart. Phys.*, 3, 055. doi:
- Skordis, C., & Złošnik, T. (2021, October), *Phys. Rev. Lett.*, 127(16), 161302. doi:
- Stark, D. V., McGaugh, S. S., & Swaters, R. A. (2009, August), *AJ*,

- 138, 392-401. doi:  
Strominger, A., & Vafa, C. (1996, February), *Physics Letters B*, 379, 99-104. doi:  
Trachternach, C., de Blok, W. J. G., McGaugh, S. S., van der Hulst, J. M., & Dettmar, R. (2009, October), *A&A*, 505, 577-587. doi:  
van der Marel, R. P., & Franx, M. (1993, April), *ApJ*, 407, 525. doi:  
Vazdekis, A., Sánchez-Blázquez, P., Falcón-Barroso, J. et al. (2010, June), *MNRAS*, 404(4), 1639-1671. doi:  
Verlinde, E. (2011, April), *Journal of High Energy Physics*, 4, 29. doi:  
Verlinde, E. (2017, May), *SciPost Physics*, 2, 016. doi:  
Watkins, L. L., Evans, N. W., & An, J. H. (2010, July), *MNRAS*, 406, 264-278. doi:  
Weijmans, A.-M., Krajnović, D., van de Ven, G., Oosterloo, T. A., Morganti, R., & de Zeeuw, P. T. (2008, February), *MNRAS*, 383, 1343-1358. doi:  
White, S. D. M. (1981, June), *MNRAS*, 195, 1037-1056. doi:  
Willmer, C. N. A. (2018, June), *ApJS*, 236(2), 47. doi:



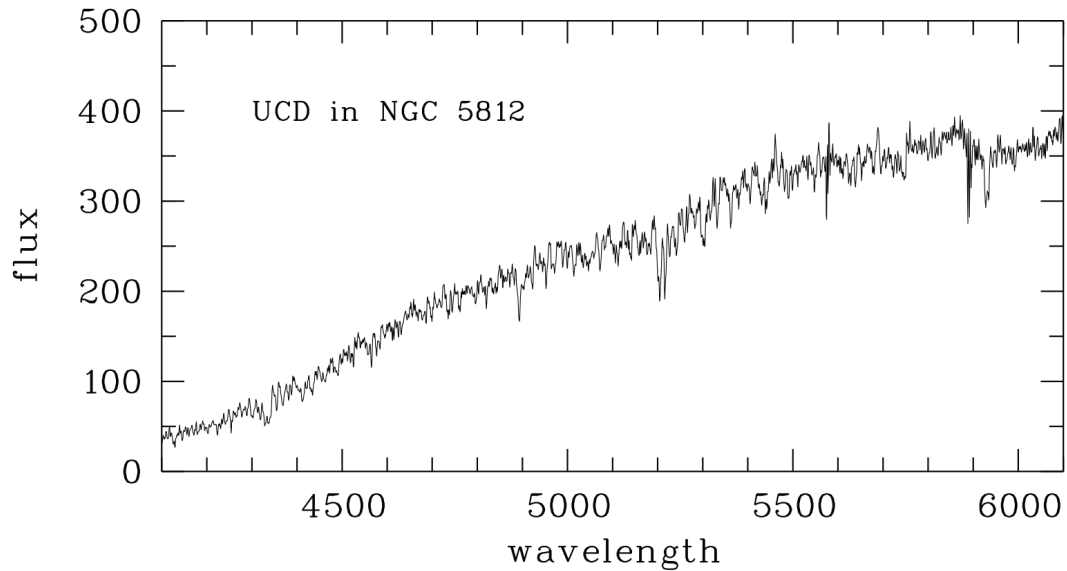
## APPENDIX A: TABLES

Table A1 lists the sample of slits of the galaxy light, for which radial velocities and velocity dispersions could be measured. The columns are the identification (the first figure is the mask number, followed by the slit number), the coordinates (J2000), the projected galactocentric distance in kpc, the heliocentric radial velocity, its uncertainty, the velocity dispersion and its uncertainty. Table A3 identifies the stars in our slit sample.

Table A2 lists the sample of GCs for which radial velocities could be measured. These are 37 measurements for 29 globular clusters and 19 stars. The columns are the identification (the first digit is the mask number, followed by the slit number), the coordinates (J2000), the heliocentric radial velocity, its uncertainty, the R-magnitude, the colour C-R.

| Id  | RA(J2000)  | Dec(J2000) | radius[kpc] | $V_r$ | error | $\sigma_{LOS}$ |       | $\sigma_{LOS}$ |       | metallicity | log(age) |
|-----|------------|------------|-------------|-------|-------|----------------|-------|----------------|-------|-------------|----------|
|     |            |            |             |       |       | 4 moments      | error | 2 moments      | error |             |          |
| 116 | 225.230398 | -7.458710  | 1.002       | 1965  | 7     | 172            | 11    | 188            | 11    | -0.01       | 1.14     |
| 19  | 225.231242 | -7.460070  | 1.416       | 1934  | 6     | 151            | 10    | 163            | 10    | -0.06       | 1.14     |
| 115 | 225.230784 | -7.455860  | 0.863       | 1974  | 4     | 191            | 8     | 210            | 8     | 0.0         | 1.16     |
| 118 | 225.233402 | -7.459140  | 1.214       | 1910  | 6     | 159            | 10    | 181            | 7.1   | -0.06       | 1.15     |
| 114 | 225.231142 | -7.453820  | 1.720       | 1919  | 6     | 153            | 11    | 161            | 5     | -0.08       | 1.15     |
| 14  | 225.233331 | -7.455870  | 0.984       | 1903  | 4.2   | 180            | 9     | 196            | 5     | -0.05       | 1.16     |
| 15  | 225.231929 | -7.451300  | 2.915       | 1924  | 4.6   | 138            | 10    | 151            | 5     |             |          |
| 122 | 225.229840 | -7.464870  | 3.846       | 1935  | 9     | 117            | 13    | 124            | 7     | -0.34       | 1.1      |
| 221 | 225.232859 | -7.455040  | 1.190       | 1931  | 6     | 172            | 10    | 191            | 6     | -0.01       | 1.16     |
| 227 | 225.227022 | -7.458690  | 2.445       | 1973  | 7     | 134            | 11    | 144            | 7.5   | -0.13       | 1.16     |
| 226 | 225.236506 | -7.452520  | 3.231       | 1905  | 6     | 108            | 10    | 115            | 8     | -0.24       | 1.16     |
| 232 | 225.239654 | -7.458670  | 3.831       | 1900  | 6.8   | 156            | 8     | 151            | 16    | -0.38       | 1.16     |
| 219 | 225.223761 | -7.459020  | 3.824       | 1998  | 8.8   | 105            | 15    | 109            | 10    | -0.2        | 1.16     |

**TABLE A1** Sample data for our galaxy spectra. The columns are: identifier (first number is the mask number, second number the slit number), coordinates, projected galactocentric distance, radial velocities and their uncertainties, velocity dispersion and their uncertainties. The coordinates are the frame WCS coordinates.



**FIGURE A1** This globular cluster has the absolute magnitude  $M_R = -12.2$ . It is old and moderately metal-poor (see section 3.5). We estimate its mass to  $1.6 \times 10^7 M_\odot$ .

| Id  | RA(J2000) | Dec(J2000) | $v_r$ (N1396) | error | $v_r$ (GC) | error | $v_r$ ( <i>final</i> ) | error | C-R  | R     | double |
|-----|-----------|------------|---------------|-------|------------|-------|------------------------|-------|------|-------|--------|
| 15  | 225.23193 | -7.45130   | 1942          | 29    |            |       | 1942                   | 29    |      |       |        |
| 16  | 225.24197 | -7.44785   | 1978          | 43    | 1909       | 41    | 1944                   | 42    | 1.42 | 22.81 |        |
| 18  | 225.24789 | -7.43559   | 1891          | 25    | 1873       | 25    | 1882                   | 25    | 1.64 | 20.34 | 213    |
| 111 | 225.23985 | -7.44285   | 1968          | 41    | 1940       | 23    | 1954                   | 33    | 1.53 | 21.48 |        |
| 117 | 225.23837 | -7.45061   | 1974          | 31    | 1955       | 37    | 1964                   | 34    | 1.47 | 21.81 | 216    |
| 119 | 225.22414 | -7.45902   | 2071          | 19    | 2053       | 19    | 2062                   | 19    | 1.70 | 21.89 | 219    |
| 120 | 225.21091 | -7.45582   | 2010          | 71    | 1990       | 47    | 2000                   | 60    | 1.88 | 21.49 |        |
| 122 | 225.22984 | -7.46487   | 1956          | 40    | 2008       | 38    | 1982                   | 39    | 1.41 | 22.51 | 230    |
| 123 | 225.23465 | -7.47690   | 1949          | 27    | 1936       | 27    | 1942                   | 27    | 1.99 | 22.16 | 235    |
| 124 | 225.21896 | -7.46620   | 1943          | 30    | 1885       | 23    | 1914                   | 27    | 1.77 | 22.55 | 238    |
| 125 | 225.22070 | -7.47564   | 2109          | 20    | 2101       | 16    | 2105                   | 18    | 1.43 | 21.81 |        |
| 126 | 225.23170 | -7.47320   | 1880          | 34    | 1889       | 32    | 1884                   | 33    | 1.17 | 22.10 |        |
| 127 | 225.21230 | -7.47584   | 1933          | 67    | 1924       | 57    | 1928                   | 62    | 1.33 | 22.50 |        |
| 128 | 225.23160 | -7.48925   | 1791          |       |            |       | 1791                   | 99    | 1.16 | 22.71 | 241    |
| 28  | 225.23492 | -7.43592   | 1545          | 90    | 1475       | 73    | 1510                   | 82    | 1.26 | 22.62 |        |
| 212 | 225.25096 | -7.43856   | 2126          | 74    |            |       | 2126                   | 74    | 1.29 | 22.97 |        |
| 213 | 225.24789 | -7.43559   | 1934          | 21    | 1926       | 28    | 1930                   | 25    | 1.64 | 20.34 | 314    |
| 216 | 225.23846 | -7.45039   | 1932          | 55    | 1904       | 58    | 1918                   | 57    | 1.47 | 21.82 |        |
| 217 | 225.23776 | -7.46174   | 2024          | 35    | 1967       | 28    | 1996                   | 32    | 1.65 | 21.26 |        |
| 219 | 225.22375 | -7.45902   | 2174          | 64    | 2127       | 52    | 2150                   | 58    | 1.69 | 21.89 |        |
| 220 | 225.22377 | -7.45532   | 2103          | 78    | 2114       | 38    | 2108                   | 61    |      |       |        |
| 222 | 225.23132 | -7.44329   | 2104          | 77    |            |       | 2104                   | 77    | 1.28 | 22.43 |        |
| 224 | 225.23109 | -7.44894   | 1742          | 68    | 1829       | 150   | 1786                   | 116   | 1.06 | 22.75 |        |
| 229 | 225.24104 | -7.45586   | 1852          | 37    | 1820       | 25    | 1836                   | 32    | 1.56 | 22.17 |        |
| 230 | 225.22984 | -7.46487   | 2067          | 51    | 2059       | 52    | 2063                   | 52    | 1.41 | 22.51 |        |
| 233 | 225.23882 | -7.46956   | 1804          | 34    | 1760       | 23    | 1782                   | 29    | 1.38 | 22.82 |        |
| 234 | 225.23547 | -7.48179   | 1946          | 70    |            |       | 1946                   | 70    | 1.48 | 22.04 |        |
| 235 | 225.23465 | -7.47690   | 2073          | 34    | 2002       | 25    | 2038                   | 30    | 1.99 | 22.16 |        |
| 236 | 225.23518 | -7.48353   | 1753          | 41    | 1742       | 50    | 1748                   | 46    | 1.03 | 22.73 |        |
| 239 | 225.24402 | -7.47851   | 1926          | 39    | 1921       | 45    | 1924                   | 42    | 1.61 | 21.85 |        |
| 240 | 225.22774 | -7.48521   | 1766          | 71    | 1740       | 73    | 1753                   | 72    |      |       |        |
| 243 | 225.21761 | -7.48575   | 1835          | 38    |            | 99    | 1417                   | 75    | 1.25 | 22.73 |        |
| 244 | 225.23170 | -7.49690   | 1985          | 44    | 1893       | 42    | 1939                   | 43    | 1.05 | 23.27 |        |
| 314 | 225.24779 | -7.43589   | 1948          | 39    | 1915       | 38    | 1932                   | 39    | 1.64 | 20.34 |        |
| 315 | 225.25200 | -7.41978   | 2027          | 56    | 1925       | 28    | 1976                   | 44    | 1.32 | 21.67 |        |
| 317 | 225.24181 | -7.42524   | 1981          | 50    | 2019       | 49    | 2000                   | 50    | 1.34 | 21.91 |        |
| 322 | 225.23480 | -7.43623   | 1790          | 60    | 1739       | 45    | 1764                   | 53    | 1.26 | 22.62 |        |

**TABLE A2** Identification (mask number and slit number), coordinates, radial velocities, C-R colours, and R-magnitude, for the globular cluster sample. The last column identifies double measurements. The coordinates are the frame WCS coordinates and for identification purposes only. The photometry is adopted from the catalogue of Lane et al. (2013).

| Id  | RA(J2000) | Dec(J2000) | $v_r$ (N1396) | error | $v_r$ (GC) | error | $v_r$ ( <i>final</i> ) | error | R    | C-R   | double |
|-----|-----------|------------|---------------|-------|------------|-------|------------------------|-------|------|-------|--------|
| 11  | 225.24913 | -7.41951   | -104          | 37    | -124       | 33    | -114                   | 35    | 1.58 | 21.56 | 22     |
| 12  | 225.22849 | -7.41639   | 1664          | 33    |            |       |                        |       |      |       | dwarf  |
| 13  | 225.26917 | -7.43612   | 9             | 28    | -14        | 36    | -2                     | 32    | 1.63 | 20.95 | 21     |
| 17  | 225.23570 | -7.43727   | 217           | 22    | 194        | 28    | 206                    | 25    | 1.26 | 20.66 |        |
| 131 | 225.23338 | -7.50151   | 103           | 25    | 89         | 30    | 96                     | 28    | 1.03 | 22.05 |        |
| 21  | 225.26917 | -7.43612   | 5             | 27    | -5         | 30    | 0                      | 29    | 1.63 | 20.95 |        |
| 22  | 225.24913 | -7.41951   | -135          | 71    | -118       | 44    | -126                   | 59    | 1.58 | 21.56 |        |
| 23  | 225.24194 | -7.42020   | 104           | 66    | 105        | 63    | 104                    | 65    | 1.18 | 19.06 | 318    |
| 211 | 225.27092 | -7.45106   | -208          | 27    | -234       | 32    | -221                   | 30    | 1.62 | 20.93 |        |
| 215 | 225.26537 | -7.43833   | -112          | 21    | -115       | 24    | -114                   | 23    | 1.36 | 21.61 | 316    |
| 223 | 225.23909 | -7.46663   | -15           | 48    | -32        | 45    | -24                    | 47    | 1.41 | 23.56 |        |
| 225 | 225.23969 | -7.45997   | 79            | 24    | 70         | 28    | 74                     | 26    | 1.33 | 21.11 |        |
| 237 | 225.21407 | -7.47114   | -27           | 33    | -42        | 22    | -34                    | 28    | 1.52 | 22.57 |        |
| 242 | 225.25816 | -7.50252   | 114           | 37    | 99         | 54    | 106                    | 46    | 1.60 | 19.51 |        |
| 246 | 225.21674 | -7.48863   | -39           | 23    | -47        | 19    | -43                    | 21    |      |       |        |
| 316 | 225.26523 | -7.43866   | -20           | 104   | -37        | 120   | -28                    | 112   | 1.36 | 21.61 |        |
| 318 | 225.24184 | -7.42052   | 118           | 58    | 84         | 52    | 101                    | 55    | 1.18 | 19.06 |        |
| 319 | 225.26250 | -7.41579   | 92            | 28    | 62         | -36   | 77                     | 32    | 1.24 | 17.38 |        |
| 320 | 225.23843 | -7.41054   | 112           | 45    | 28         | 38    | 70                     | 42    | 1.04 | 22.05 |        |

**TABLE A3** Identification(mask number and slit number), coordinates, radial velocities, C-R colours, R-magnitudes for the stars in our sample. Object 12 is the dwarf companion. The coordinates are for identification purposes only. The photometry is adopted from the catalogue of Lane et al. (2013).